Published in final edited form as:
Neurobiol Aging. 2008 October ; 29(10): 1563–1575. doi:10.1016/j.neurobiolaging.2007.03.022.

An MRI study of age-related white and gray matter volume changes in the rhesus monkey

Jonathan J. Wisco[1], **Ronald J. Killiany**[1], **Charles R. G. Guttmann**[2], **Simon K. Warfield**[2,3,4], **Mark B. Moss**[1,5], and **Douglas L. Rosene**[1,5]

1*Laboratory for Cognitive Neurobiology, Department of Anatomy and Neurobiology, Boston University School of Medicine, Boston, MA 02118*

2*Center for Neurological Imaging, Department of Radiology, Brigham and Women's Hospital, Harvard Medical School, Boston, MA 02115*

3*Computational Radiology Laboratory, Department of Radiology, Brigham and Women's Hospital, Harvard Medical School, Boston, MA 02115*

4*Computational Radiology Laboratory, Departments of Radiology, Children's Hospital and Brigham and Women's Hospital, Harvard Medical School, Boston, MA 02115*

5*Yerkes National Primate Research Center, Emory University, Atlanta, GA 30322, USA*

Abstract

We applied the automated MRI segmentation technique Template Driven Segmentation (TDS) to dual-echo spin echo (DE SE) images of eight young (5–12 years), six middle-aged (16– 19 years) and eight old (24–30 years) rhesus monkeys. We analyzed standardized mean volumes for 18 anatomically defined regions of interest (ROI's) and found an overall decrease from young to old age in the total forebrain (5.01%), forebrain parenchyma (5.24%), forebrain white matter (11.53%) forebrain gray matter (2.08%), caudate nucleus (11.79%) and globus pallidus (18.26%). Corresponding behavioral data for five of the young, five of the middle-aged and seven of the old subjects on the Delayed Non-matching to Sample (DNMS) task, the Delayed- Recognition Span Task (DRST) and the Cognitive Impairment Index (CII) were also analyzed. We found that none of the cognitive measures were related to ROI volume changes in our sample size of monkeys.

Keywords

Aging; rhesus monkey; MRI; white matter; gray matter; cerebral cortex; Template Driven Segmentation (TDS); normal aging

1. Introduction

In selecting an appropriate animal model in which to study the effects of normal aging, the most important criteria that must be met is how closely the animal model reflects human

Corresponding author (present address) Jonathan J. Wisco, Ph.D., Department of Pathology and Laboratory Medicine, David Geffen School of Medicine at UCLA, 10833 Le Conte Ave., Room 52-060 CHS, Los Angeles, CA. 90095-1732, Phone: 310-825-7880, Fax: 310-825-3058, E-mail: jjwisco@mednet.ucla.edu.

neurobiology. The rhesus monkey (Macaca mulatta) qualifies as an excellent non-human primate model for the study of normal aging for several reasons. First, the anatomy of the brain more closely resembles that of the human brain than other available laboratory animals. Second, unlike the human brain, the rhesus monkey brain does not exhibit the characteristic neuropathological loss of neurons that characterizes Alzheimer's disease [41] and hence normal aging can be studied without risk of intrusion of AD cases into the sample. Third, the life span of the human compared to the rhesus monkey approximately follows a ratio of 3:1 [6,57]; Based on this, monkeys age 5 to 12 years are considered "young adults", those between 13 and 19 are considered middle aged and those beyond 20 years are considered "aged adults" [40]. Fourth, monkeys can be evaluated on batteries of behavioral tasks that tap cognitive domains that clearly correspond to human cognitive functions [16]. Fifth, monkeys and humans show similar patterns of age-related cognitive changes [35].

Studies of human aging post-mortem have been faced with the difficult problem of obtaining optimally prepared brain tissue from behaviorally well-characterized subjects. Recent advances in MRI technology, however, have allowed *in vivo* anatomical assessments to be conducted with closely monitored human subjects. These studies of the human brain have reported a variety of age-related changes in the volumes of different tissue components and have reported loss of gray matter, loss of white matter and loss of both [5,7,9,13,14,18,20,23, 29,30,48–53]. For example, using manual tracing methods, Raz et al. [49,51] reported gray matter and white matter volume decrease in the prefrontal cortex and medial temporal lobe from high resolution spoiled gradient recalled (SPGR) images and Bartzokis et al. [5] reported gray matter volume loss in the frontal and temporal lobes accompanied by a quadratic (increase then decrease) change of white matter volume with increasing age in the same lobes from dual-echo spin echo images. However, using automated segmentation methods, Guttmann et al. [14] reported white matter volume decrease, with a minor change in gray matter volume on dual-echo spin echo images, and Ge et al. [9] reported total gray and white matter volume loss with age in both men and women on dual-echo fast spin echo images.

Studies involving the rhesus monkey as an animal model for normal aging have focused on behavioral [2,3,16,24,25,27,31–33,36,37,45–47] and anatomical [1,28] endpoints, but few have examined both [40–42]. The rhesus monkey model provides the opportunity to study age-related brain structural changes using MRI with the assurance that Alzheimer's disease pathology will not confound the interpretation of results. Unfortunately unlike human aging studies, only a handful of rhesus monkey studies have utilized structural MRI analysis for the study of aging.

For example, Andersen et al. [1] used a signal intensity classification algorithm to segment female monkey brains into gray matter, white matter and cerebrospinal fluid (CSF) classes. They found a decrease in parenchyma volume (normalized to the intracranial cavity volume). Andersen and colleagues attributed the decline in parenchyma volume to a decrease in gray matter volume and a compensatory increase in CSF volume, with some white matter volume loss up to 15 years of age. However, for later years of the monkeys' lives, they attributed parenchyma volume loss mostly to white matter volume loss.

In another example, Matochik et al. [28] used a manual tracing segmentation method to measure the volume of the rhesus monkey striatum. In 19 male monkeys between the ages of 3 and 30 years, they found age-related declines in normalized caudate nucleus and putamen volumes when comparing young, middle-aged and aged groups. Matochik and colleagues postulated that the volume loss could be due to both neuronal- and non-neuronal-related atrophy [28, 34].

The rhesus monkey model of normal aging also provides the opportunity to study cognitive decline [2,3,16,24,27,31–33,36,37,40–42,45–47] using behavioral tasks that are similar to clinical tests [4,8,25,44]. Similar to anatomical studies, the advantage of using the rhesus monkey as an animal model for cognitive decline in normal aging is the absence of Alzheimer's Disease-associated cognitive impairment.

The goal of this investigation was to utilize MRI methods to determine if there are age-related changes in the major components of the forebrain in behaviorally characterized monkeys participating in ongoing investigations of normal aging [16,24,32,33,36,37,40–42]. To accomplish this efficiently we applied the automated MRI segmentation technique Template Driven Segmentation (TDS) to legacy rhesus monkey MRI data. The technique has been validated in human studies of normal aging [15,17,58,59]. We created a rhesus monkey anatomical atlas template for the segmentation pipeline to ensure that all voxels were assigned to anatomically validated components. Age-related volume changes calculated by TDS were then compared to cognitive performance as measured by the Delayed Non-Matching to Sample (DNMS), the Delayed Recognition Span Task (DRST) and the Cognitive Impairment Index (CII), which is a composite score of DNMS acquisition, DNMS 2-minute delay and DRST spatial condition tasks. The underlying hypothesis for this investigation was that age-related brain structure volume decreases would be associated with impaired cognitive performance.

2. Materials and Methods

2.1. Selection of animal subjects and housing accommodations

A total of 22 male rhesus monkeys were selected for this study, eight of whom were young (5–12 years), six of whom were middle-aged (16–19 years) and eight of whom were old (24–30 years) at the time of MRI scan acquisition. All subjects were selected from the rhesus monkey population at the Yerkes National Primate Research Center (YNPRC) according to explicit criteria which excluded subjects with histories that included any of the following: splenectomy or thymectomy, exposure to radiation, organ transplantation, malnutrition, cancer, chronic illness, chronic drug administration or any neurological disease. Prior to entry into the study, all animals received a medical examination that included serum chemistry, hematology, urine analysis and fecal analysis as well as assessment of visual function to ensure that behavioral testing would not be impeded. Once accepted, quarterly physicals were conducted to ensure continued health.

While participating in the study, all monkeys were housed first at YNPRC and subsequently transferred to the Laboratory Animal Science Center at Boston University Medical Center (BUMC) where they were individually housed within auditory and visual range of other monkeys. They were all maintained on a normal diet consisting of Standard Purina Monkey Chow and under a 12-hour light/dark cycle consisting of a gradual transition of one hour. Feeding occurred once a day following behavioral testing, and water was available continually. The monkeys were also inspected visually on a daily basis by both animal care personnel and research technicians. All procedures were approved by the Institutional Animal Care and Use Committees (IACUC) of both YNPRC and BUMC. In addition both YNPRC and BUMC are fully accredited by the Association for the Assessment and Accreditation of Laboratory Animal Care (AAALAC) and all procedures conformed to the NIH Public Health Service Policy on Humane Care and Use of Laboratory Animals.

2.2. Imaging protocol

Monkeys were anaesthetized using a mixture of ketamine and xylazine for transport from the colony room to the MR scanner. Upon arrival, monkeys were placed in a 1.5T Signa GE scanner bore in the prone position, their heads stabilized in a non-ferrous stereotactic frame using raised

eye and ear bars [55]. The ear bars marked the zero coordinate of the coronal plane. A 5- inch surface coil was then secured directly over the cranium, parallel to the horizontal axis of the stereotactic frame. The raised ear and eye bars placed the center of the forebrain approximately within the center of the surface coil as well as the bore of the scanner. Anesthesia level was monitored and maintained with supplementary doses for the duration of the image acquisition.

A localizer Fast Spin-echo (FSE) scan [TR = 2000 ms; TE = 90 ms; 5.0 mm slice; FOV = 256 × 192; 1 nex] was acquired in the sagittal plane to assist with the orientation of the subsequent scan protocol. Interleaved dual-echo spin-echo (DE SE) sequences TR = 3000 ms; TE = 30/80 ms; 2.7 mm slice; FOV = 15 × 15 mm (256 ×256); 1 nex] yielding alternating proton density weighted (pdw) and T2-weighted (t2w) images were acquired in the coronal plane. The series consisted of approximately 60 images (30 pdw, 30 t2w) covering the entire rostral to caudal extent of the brain. Anisotropic diffusion filtering was applied to the DE SE images to improve signal to noise ratio while preserving structure edges [10].

2.3. Creation of a reference atlas

A reference label atlas of the monkey brain was constructed by manual outlining of DE SE images of AM093 using 3D Slicer (www.slicer.org) after anisotropic diffusion filtering. The resulting atlas consisted of 14 manually segmented ROI's: forebrain white matter, cerebral cortex, caudate nucleus, putamen, globus pallidus, claustrum, thalamus, hypothalamus, brainstem, cerebellum, lateral ventricles, third ventricle, cerebral aqueduct and fourth ventricle. Operational definitions for the segmented ROI's can be found in the Appendix.

Although the pdw images provided good contrast between gray matter and white matter regions, and the T2w images provided good contrast between brain and CSF, Nissl stained histological sections from AM093, digitized using the Inquiry digitizing system (Loats Associates, Inc.), and a published histological atlas [39], served as anatomical references for correctly labeling each ROI and for distinguishing low contrast brain structures on the DE SE images. The atlas was validated by four additional independent raters who identified the same 14 ROI's on the DE SE images of the atlas subject ($P = 0.4664$, repeated measures ANOVA).

An intracranial cavity (ICC) ROI [14,21,58,59] was created using the label threshold function in 3D Slicer and included the entire cerebrum, cerebellum and brainstem (up to the most inferior margin of the cerebellum). ICC volumes were not significantly different between age groups [$F(2,19) = 0.79$, $P = 0.4699$]. The ICC ROI volume was used to standardize all other ROI volumes. The ICC ROI was also used as the reference matrix for the first of the two registration steps in the non-linear registration algorithm described subsequently.

2.4. Segmentation procedure for subjects

DE SE brain images of all 22 monkeys were segmented using an automated pipeline with minimal rater intervention (Figure 1). First, anisotropic diffusion filtering smoothed the images. Second, an intracranial cavity (ICC) ROI [14,21,58,59] was created. Third, a data set statistically segmented for gray matter, white matter and cerebrospinal fluid (CSF) was generated using the 3D Expectation-Maximization (3D EM) algorithm, which has been described previously [60,61]. Fourth, Template Driven Segmentation (TDS) [15,17,58,59] parcellated the gray matter and CSF further into anatomically defined regions based on a reference label atlas created specifically for this data set.

TDS accomplished the anatomical segmentation by first performing a linear transformation of the reference ICC to the subject ICC (for this step of the segmentation pipeline, the reference data set was the input, and the subject data sets were the target). The resulting transformation matrix was then applied to the reference atlas so that it was now also linearly registered with

the subject ICC and 3D EM segmented data set. Finally, TDS performed a non-linear, elastic matching registration of the reference atlas to the 3D EM segmented data set to anatomically classify each voxel. This pipeline was repeated for each subject.

The results provided further segmentation of the gray matter, white matter and CSF regions into more specific regions of interest (ROI) contained in the template atlas. ROI's of total forebrain (sum of white matter, gray matter and ventricles, but not subarachnoid CSF around the brain or in sulci, fissures and cisterns), forebrain parenchyma (sum of white matter and gray matter), forebrain gray matter (sum of cerebral cortex, caudate nucleus, putamen, globus pallidus, claustrum, thalamus, hypothalamus), and ventricular cerebrospinal fluid (sum of lateral ventricles, third ventricle, cerebral aqueduct and fourth ventricle) were derived.

2.5. Behavioral testing

Five of the young, five of the middle-aged and seven of the old subjects whose brains were imaged also had behavioral testing data available from a battery of cognitive tasks assessing learning and memory as part of ongoing studies. We matched the behavioral data as close to the date of imaging as possible, resulting in a mean date difference of 1 year for young and middle-aged monkeys and 3 years for old monkeys. For all three age groups, the date difference was within the group age range (i.e. behavioral data for old monkeys was not acquired while they were middle-aged). A summary of behavioral tasks is shown in Table 1.

The tasks included the Delayed Non-Matching to Sample (DNMS) task (acquisition, 2- minute delay and 10-minute delay conditions) and the Delayed Recognition Span Task (DRST) (spatial and object conditions). The details of these tasks and the changes associated with normal aging in our monkeys have been presented in detail in Herndon et al. [16] and will only be summarized briefly here.

The tasks were given to all subjects in a fixed order beginning with the acquisition condition of the DNMS task. In the acquisition phase there was a 10 second delay between the presentation of a trial unique sample stimulus and a choice trial where the sample object was paired with a novel object. This assessed the monkey's ability to learn the non-match rule in which the novel object must be identified and chosen to receive a reward. After learning was achieved by performing at a criterion of 90% correct over 100 trials, the DNMS delay phase was given to assess recognition memory over time. In this phase animals were tested for 100 trials with a delay between sample object presentation and choice trial of 120 seconds (2 minutes) and this was followed by another 100 trials with a delay of 600 seconds (10 minutes).

After completion of DNMS training and testing, animals were tested on the Delayed Recognition Span Task (DRST), which assessed the animals' working memory capacity in both the spatial and object modalities. For the spatial DRST condition, identical black plaques were used as stimuli on an 18 well board. On the first trial one plaque was presented in one of the 18 locations and covered the reward. On the second trial, with the location of the first plaque unchanged, a new plaque was added over a new baited location and the monkey must use the non-match rule to pick the new plaque to obtain a reward. On subsequent trials, new plaques were added over a new location until an error was made. In the object condition of the task, the same novelty rule applied as new objects were sequentially added, but the spatial position of all objects on the board varied from trial to trial so that object features are the only cue. The number of objects was increased trial to trial until an error was made.

We also calculated the Cognitive Impairment Index (CII), which was a composite score of DNMS acquisition, DNMS 2-minute delay and DRST spatial condition tasks. Higher CII scores indicated greater cognitive impairment.

2.6. Data analysis

For each subject, ROI volumes were normalized by dividing the ROI volume by the ICC volume. These normalized volumes were used for all statistical analyses such that "ROI volume" always refers to a standardized measure.

We analyzed the relationship of each ROI volume (total forebrain, forebrain parenchyma, forebrain white matter, forebrain gray matter, cerebral cortex, caudate nucleus, putamen, globus pallidus, claustrum, thalamus, hypothalamus, brainstem, cerebellum, ventricular cerebrospinal fluid, lateral ventricles, third ventricle, cerebral aqueduct and fourth ventricle) with age as a between groups factor for one-way ANOVA, then followed up with Bonferroni *a posteriori* comparisons.

We also analyzed the relationship of those ROI volumes shown to be significantly associated with age group with individual performance on the DNMS task, DRST and the CII using multiple regression. For these analyses, performance on each behavioral task was the outcome variable and ROI volume and age (linear and non-linear) were predictor variables. All calculations were performed by the statistical software package, Stata 8.2 (Stata Corp, College Station, TX).

3. Results

3.1. ROI volume as a function of age group

One-way ANOVA analysis revealed a significant overall main effect of age group for the following standardized ROI volumes (Figure 2): total forebrain [$F(2,19) = 20.76$, $P < 0.0001$], forebrain parenchyma [$F(2,19) = 20.40$, $P < 0.0001$], forebrain white matter [$F(2,19) = 12.89$, $P = 0.0003$], forebrain gray matter [$F(2,19) = 3.96$, $P = 0.0365$], caudate nucleus [$F(2,19) = 11.48$, $P = 0.0005$], globus pallidus [$F(2,19) = 5.39$, $P = 0.0140$] and third ventricle [$F(2,19) = 4.53$, $P = 0.0247$, data not shown]. Cerebral cortex [$F(2,19) = 0.76$, $P = 0.4800$] and putamen [$F(2,19) = 1.40$, $P = 0.2700$] volumes were not found to be significantly different between age groups.

Follow-up *a posteriori* analyses for total forebrain showed a trend toward significant mean volume increase from young to middle-age ($P = 0.086$), a significant decrease from young to old age ($P = 0.001$) and a significant decrease from middle-age to old age ($P < 0.001$).

Forebrain parenchyma showed a trend toward significant mean volume increase from young to middle-age ($P = 0.099$), a significant decrease from young to old age ($P = 0.001$) and a significant decrease from middle-age to old age ($P < 0.001$).

Forebrain white matter showed a significant mean volume decrease from young to old age ($P = 0.009$) and a significant decrease from middle-age to old age ($P < 0.001$).

Forebrain gray matter showed a significant mean volume decrease from middle-age to old age ($P = 0.038$).

Caudate nucleus showed a significant mean volume increase from young to middle-age ($P = 0.017$) and a significant decrease from middle-age to old age ($P < 0.001$).

Globus pallidus showed a significant mean volume decrease from middle-age to old age ($P = 0.014$).

Third ventricle (data not shown) showed a significant mean volume increase from middle-age to old age ($P = 0.023$).

Mean (SE) values for all ROI's for each age group are included in Table 2.

3.2. Cognitive performance as a function of ROI volume and age

We did not find a significant relationship between total forebrain, forebrain parenchyma, forebrain white matter, caudate nucleus or globus pallidus ROI volumes with performance on the Delayed Non-Matching to Sample (DNMS) task, Delayed Recognition Span Task (DRST) or with the Cognitive Impairment Index (CII). Mean (SE) values of the behavioral measures for each age group are included in Table 1.

4. Discussion

4.1. Summary of results

We have reported two principal results. First, there was a significant age-related decrease in the ROI volumes of total forebrain, forebrain parenchyma, forebrain white matter, forebrain gray matter, caudate nucleus and globus pallidus. We also found a significant increase in third ventricle volume, but the volume changes were less than 0.2 cc. Volume changes this small could be accounted for by partial volume effects, and so further analysis was not done for this ROI. Second, none of the ROI volumes significant with age group were associated with cognitive performance on the Delayed Non-Matching to Sample (DNMS) task, Delayed Recognition Span Task (DRST) or the Cognitive Impairment Index (CII).

4.2. Volume changes

To our knowledge, the present study uniquely examines ROI volume changes of the entire rhesus monkey forebrain, brainstem and cerebellum as a function of age group. The overall decrease from young to old age in the standardized volumes of total forebrain (5.01%), forebrain parenchyma (5.24%), forebrain white matter (11.53%) forebrain gray matter (2.08%), caudate nucleus (11.79%) and globus pallidus (18.26%) that we found have been similarly reported by many human aging studies [1,5,9,13,14,18,20,22,23,28,30,38,48,50,52, 53].

Forebrain white matter and forebrain gray matter volume changes in the monkey closely matches the results of Guttmann and colleagues [14] and Ge and colleagues [9] in humans. We were surprised, however, to find that ventricular CSF volume did not increase significantly with age since the phenomenon has been established as a marker for normal aging in humans [43,56]. CSF volume increase has also been characterized in the rhesus monkey by Andersen and colleagues, [1], but their measure included both cortical surface CSF and ventricular CSF. In our sample size, ventricular CSF accounted for only 2.6 percent of the total brain volume and increased 3 percent (0.1 percent of ICC) from young to old age. With a 5 percent decrease in total brain volume (4 percent of ICC), only cortical surface CSF increases could balance the loss of brain parenchyma within the ICC. Unfortunately in the present study, we only included ventricular CSF in the template atlas, concerned with the possibility that sulcal CSF would not segment correctly due to partial volume effects. We will need to revisit this issue in order to make a more accurate assessment of total CSF volume changes. Another possibility for the discrepancy between our results and the human data concerns the sample size of 8 young, 6 middle-aged and 8 old monkeys. Our small sample size may not have enough statistical power to detect small changes in rhesus monkey ventricular volume.

Although we found a decrease in cerebral cortical volume as a function of age group, that change was not statistically significant ($P = 0.4800$). Cortical volume loss has been reported in human studies, however [5,49,51,53]. Whereas the studies by Bartzokis and colleagues and Raz and colleagues focused on regional areas of cerebral cortex (notably frontal and temporal lobes), our study examined the entire cerebral cortex. It is possible that, when analyzed together,

significant decreases in the cortical volume of selective areas are washed out by other areas of the cortex that experience little or no changes in volume. Indeed, Salat and colleagues [54] found non-significant differences in global cortical thinning, but follow-up regional analysis of the primary and secondary cortical areas showed significant differences between young and old subjects. Had we parcellated our template atlas to include regional areas of cerebral cortex, we might have found similar results that have been reported by Bartzokis, Raz and their colleagues.

The overall decrease in caudate nucleus and globus pallidus agrees in part with the results reported in humans [13,38,48,50] and in monkeys [28]. The basal ganglia have extensive connections with the prefrontal, temporal and parietal association cortices as well as the thalamus [11,12,62,63]. To determine whether volume changes in forebrain and basal ganglia regions could be age-related, we performed follow-up multiple regression analyses of caudate nucleus and globus pallidus as outcome variables of forebrain white matter, forebrain gray matter (separately) and age (quadratic fit) as predictor variables. Forebrain white matter and forebrain gray matter predicted caudate nucleus volume (but not globus pallidus volume) at trends towards significance of $P = 0.057$, $P = 0.068$, respectively. Again, the age-related relationship between forebrain and basal ganglia ROI volumes may have reached significance had we restricted our analysis to specific lobes. Nevertheless, these results suggest that forebrain and subcortical volumes are age-related. A diffusion tensor imaging study of the subcortical white matter may reveal whether fiber tract integrity also changes with age.

Unlike the study by Matochik and colleagues [28], we did not observe a significant decrease in putamen ROI volume even though we were able to corroborate the decrease in caudate nucleus volume. In the present study, we attempted to delineate the claustrum from the lateral edge of the putamen. Partial volume effects at the interface between the two nuclei could easily have affected the calculation of the putamen during the automated segmentation process. Matochik and colleagues do not address whether the claustrum may have influenced their delineation of the putamen. We are not aware of any other rhesus monkey studies of putamen volume that could shed light on the discrepant findings.

We observed an increase in forebrain white matter and forebrain gray matter volume from young to middle-age, followed by a decrease from middle-age to old age in our sample set of monkeys (Figure 2), corroborating observations made by Bartzokis and colleagues [5] in human subjects. We examined whether this pattern of volume change was true for cerebral cortex, caudate nucleus, putamen, globus pallidus, claustrum, thalamus and hypothalamus ROI's, the components of the forebrain gray matter ROI. Indeed, the growth pattern was observed for all of the ROI's except thalamus and hypothalamus, which remained steady in volume through increasing age (data not shown). It is possible that this phenomenon could be caused by a sampling error of larger brains in the middle-aged group, but we verified that the brain weights (measured by water displacement) of the monkeys were only slightly, but not significantly, greater than the monkeys of the other cohorts [16]. Another confounding source could be in the segmentation of the tissue classes at the gray/white interface. Since the voxel dimensions in the legacy MRI data were quite large, partial volume effects may have played a role. However, the fact that almost every ROI experienced quadratic volume change leads us to believe that our results may be biological. Bartzokis and colleagues [5] attribute the volume changes of white matter relative to gray matter in the frontal and temporal lobes to the timing of myelination and degeneration, respectively, from the second through the fourth decade of life in humans. In post-mortem observations, Kemper [19] noted an increase in myelination of the association fibers through childhood and adolescence, steadying in early middle-age, then decreasing in late middle-age to old age; Lintl and Braak [26] reported decreased myelin staining in the visual cortex stripe of Gennari beginning in the third decade of life of normal subjects.

4.3. Cognitive assessment

Changes in total forebrain, forebrain parenchyma, forebrain white matter, forebrain gray matter, caudate nucleus and globus pallidus ROI volumes were not related to cognitive performance on the DNMS task, DRST or the CII. In previous studies, however, we and our colleagues have shown a relationship between cognitive decline on recognition memory tasks [3,16,27,31,36,37,41,45–47]. We believe that the discrepancies between the present and previous results were due to several sources. First, our ROI's included both hemispheres and spanned the entire forebrain. More specific ROI's within white matter (and in the gray matter) regions, such as "medial temporal lobe subcortical white matter," may be related to cognitive performance. However, accurate demarcation of the white matter fibers would require diffusion-weighted data that was not acquired with these monkeys. This endeavor is worth pursuing for future studies. Second, the available behavioral data for the monkeys was incomplete for some tasks, particularly in the middle-aged group. A better-controlled sample size and/or a longitudinal study might be able to provide the necessary statistical power to determine the relationship between cognitive decline on recognition memory tasks and brain volumes.

4.4. Caveats

The demarcation of ROI's between voxels corresponding to different tissue classes should always be taken with some caution. We readily acknowledge that statistical and anatomical segmentation of brain structures, particularly for the image quality used in our study, will be influenced by partial volume effects.

Acknowledgements

This research was funded in part by the following grants: NIH grants F31-AG05897, P01-AG00001, P41-RR13218-01, P51-RR-00165, R01-NS35142, R37-AG17609 and R21 MH067054, Boston University School of Medicine Graduate Student Research Fellowship and National Multiple Sclerosis Society grant RG 3478A2/2. No authors had any conflict of interest with the work presented in this paper.

The authors would like to thank Svetlana Egorova, Ying Wu, Zsusanna Liptak and Jeremy Warner for their assistance with the validation of the template atlas.

Appendix

The DE SE data were acquired over a 10-year period using a single set of sequence parameters that were optimized at the beginning of the study. Due to the anisotropic voxel dimensions, data were best viewed in the coronal plane. Cerebral cortex, forebrain white matter and lateral ventricles were easily distinguishable in this orientation. However, operationally defined landmarks assisted with the parcellation of the thalamus, hypothalamus, third ventricle, cerebral aqueduct, fourth ventricle, brainstem and cerebellum.

6.1. Operationally defined landmarks

The following landmarks were overlaid on the images of the atlas subject to guide the creation of the ROI's (Figure A1).

Caudate-Putamen landmark

A line parallel to the internal capsule, separating the caudate medially from the putamen laterally where they are connected anteriorly by the nucleus accumbens. The nucleus accumbens is therefore distributed evenly (approximately) between the caudate and putamen.

Third ventricle landmark

An axial line just inferior to the body of the fornix.

Thalamus-Hypothalamus landmark

A line that extended from the vertical midpoint of the third ventricle to the most dorsal aspect of the hippocampus. This line was placed on slices where both the thalamus and hypothalamus were adjacent to each other.

Thalamus-Brainstem landmark

A line that extended from the most inferior point of the third ventricle to the most dorsal aspect of the hippocampus. This landmark was never present on the same image slice as the thalamus-hypothalamus landmark.

Lateral ventricle landmark

A line tangential to the lateral corner of the lateral geniculate nucleus of the thalamus. This landmark defined the medial border of the inferior horn of the lateral ventricles where the choroidal fissure was difficult to identify.

Brainstem-Cerebellum landmark

A parasagittal line along the lateral edge of the brainstem. Bilaterally, these two parallel lines would differentiate the brainstem from the cerebellum on image slices rostral to the appearance of the fourth ventricle such that brainstem is labeled between the lines, and the cerebellum is labeled outside the lines.

Fourth ventricle landmark

A line extended from the lateral corner of the fourth ventricle to the angle between the cerebellum folia and the brainstem. The landmark appeared on the first image slice where the fourth ventricle can be seen between the brainstem and cerebellum.

6.2. Operationally defined structures and regions

The following operational definitions for ROI's guided the creation of the atlas after operationally defined landmarks were overlaid on the images.

Intracranial Cavity (ICC)

Included all pixels of the brain parenchyma and cerebrospinal fluid except the olfactory tract and the optic nerve rostral to the optic chiasm, and the brainstem inferior to the cerebellomedullary cistern.

Total forebrain

Included forebrain white matter, forebrain gray matter and ventricles.

Forebrain parenchyma

Included forebrain white matter and forebrain gray matter.

Forebrain white matter

Included all white matter of the cerebral hemispheres but not white matter contained within the deep gray matter structures of the basal ganglia, brainstem or cerebellum.

Forebrain gray matter

Included the cerebral cortex, caudate nucleus, putamen, globus pallidus, claustrum, thalamus and hypothalamus, but not the brainstem and cerebellum.

Cerebral cortex

Included cerebral cortex, basal forebrain, hippocampus and amygdala, but not nuclei of the deep gray matter.

Caudate Nucleus

Striatal gray matter medial to the Caudate-Putamen landmark, (including the medial portion of nucleus accumbens) extending throughout the body and tail.

Putamen

Striatal gray matter lateral to the Caudate-Putamen landmark (including the lateral portion of nucleus accumbens).

Globus Pallidus

Lenticular nucleus gray matter including internal and external segments, but not including the putamen.

Claustrum

Deep gray matter between putamen and insula surrounding external capsule and extending partially into the temporal stem white matter.

Thalamus

First visible posterior to the optic chiasm, one slice caudal to the first slice on which the hypothalamus first appeared. The thalamus was distinguished from the hypothalamus by the thalamus-hypothalamus landmark. Caudal to the hypothalamus, the thalamus was distinguished from the brainstem by the thalamus-brainstem landmark.

Hypothalamus

First visible on the slice which exhibited the anterior commissure traversing across the midline. On this image the HYP was inferior to the anterior commissure. The thalamus and hypothalamus were distinguished by the thalamus-hypothalamus landmark.

Brainstem

Included all intrinsic white matter and gray matter demarcated by the thalamus-brainstem, brainstem-cerebellum and fourth ventricle landmarks. The brainstem was excluded on images caudal to the section where the cerebellomedullary cistern and fourth ventricle appear continuously.

Cerebellum

Included all intrinsic white matter and gray matter structures demarcated by the brainstem-cerebellum and fourth ventricle landmarks and its interface with subarachnoid CSF and cerebral cortex. The fourth ventricle was not included.

Ventricular CSF

Sum of ventricular volumes.

Lateral ventricles

Included all CSF-associated pixels within the anterior horns, confluence, posterior horns and inferior horns. The lateral ventricle landmark was the medial border for the inferior horns.

Third ventricle

Included all CSF-associated pixels within the diencephalon, extending rostrally between the hemi-structures of the hypothalamus and caudally between the hemispheres of the posterior thalamus up to the transverse fissure. The superior border of the third ventricle was the third ventricle landmark.

Cerebral aqueduct

Included all CSF-associated pixels leading from the third ventricle to the fourth ventricle at the midline of the brainstem.

Fourth ventricle

Included the CSF-associated pixels just caudal to the cerebral aqueduct, between the cerebellum and brainstem as demarcated by the fourth ventricle line, not including the cerebellomedullary cistern.

References

1. Andersen AH, Zhang Z, Zhang M, Gash DM, Avison MJ. Age-associated changes in rhesus CNS composition identified by MRI. Brain Res 1999;829(1– 2):90–98. [PubMed: 10350533]
2. Bachevalier J, Mishkin M. Mnemonic and neuropathological effects of occluding the posterior cerebral artery in Macaca mulatta. Neuropsychologia 1989;27(1):83–105. [PubMed: 2710318]
3. Bachevalier J, Landis LS, Walker LC, Brickson M, Mishkin M, Price DL, Cork LC. Aged monkeys exhibit behavioral deficits indicative of widespread cerebral dysfunction. Neurobiol Aging 1991;12 (2):99–111. [PubMed: 2052134]
4. Barbeau EJ, Felician O, Joubert S, Sontheimer A, Ceccaldi M, Poncet M. Preserved visual recognition memory in an amnesic patient with hippocampal lesions. Hippocampus 2005;15(5):587–596. [PubMed: 15884094]
5. Bartzokis G, Beckson M, Lu PH, Nuechterlein KH, Edwards N, Mintz J. Age-related changes in frontal and temporal lobe volumes in men: a magnetic resonance imaging study. Arch Gen Psychiatry 2001;58 (5):461–465. [PubMed: 11343525]
6. Bowden DM, Williams DD. Aging. Adv Vet Sci Comp Med 1984;28:305–341. [PubMed: 6395674]
7. Condon B, Patterson J, Wyper D, Hadley D, Grant R, Teasdale G, Rowan J. Use of magnetic resonance imaging to measure intracranial cerebrospinal fluid volume. Lancet 1986;1(8494):1355–1357. [PubMed: 2872473]
8. Dickerson BC, Salat DH, Bates JF, Atiya M, Killiany RJ, Greve DN, Dale AM, Stern CE, Blacker D, Albert MS, Sperling RA. Medial temporal lobe function and structure in mild cognitive impairment. Ann Neurol 2004;56(1):27–35. [PubMed: 15236399]
9. Ge Y, Grossman RI, Babb JS, Rabin ML, Mannon LJ, Kolson DL. Age-related total gray matter and white matter changes in normal adult brain. Part I: volumetric MR imaging analysis. AJNR Am J Neuroradiol 2002;23(8):1327–1333. [PubMed: 12223373]
10. Gerig G, Kubler O, Kikinis R, Jolesz FA. Nonlinear anisotropic filtering of MRI data. IEEE Transactions on Medical Imaging 1992;(11):221–232. [PubMed: 18218376]
11. Graybiel AM. The basal ganglia. Curr Biol 2000;10(14):R509–R511. [PubMed: 10899013]
12. Graybiel AM. Network-level neuroplasticity in cortico-basal ganglia pathways. Parkinsonism Relat Disord 2004;10(5):293–296. [PubMed: 15196508]
13. Gunning-Dixon FM, Head D, McQuain J, Acker JD, Raz N. Differential aging of the human striatum: a prospective MR imaging study. AJNR Am J Neuroradiol 1998;19(8):1501–1507. [PubMed: 9763385]

14. Guttmann CR, Jolesz FA, Kikinis R, Killiany RJ, Moss MB, Sandor T, Albert MS. White matter changes with normal aging. Neurology 1998;50(4):972–978. [PubMed: 9566381]

15. Guttmann CR, Kikinis R, Anderson MC, Jakab M, Warfield SK, Killiany RJ, Weiner HL, Jolesz FA. Quantitative follow-up of patients with multiple sclerosis using MRI: reproducibility. J Magn Reson Imaging 1999;9(4):509–518. [PubMed: 10232508]

16. Herndon JG, Moss MB, Rosene DL, Killiany RJ. Patterns of cognitive decline in aged rhesus monkeys. Behav Brain Res 1997;87(1):25–34. [PubMed: 9331471]

17. Iosifescu DV, Shenton ME, Warfield SK, Kikinis R, Dengler J, Jolesz FA, McCarley RW. An automated registration algorithm for measuring MRI subcortical brain structures. Neuroimage 1997;6 (1):13–25. [PubMed: 9245652]

18. Jernigan TL, Archibald SL, Berhow MT, Sowell ER, Foster DS, Hesselink JR. Cerebral structure on MRI, Part I: Localization of age-related changes. Biol Psychiatry 1991;29(1):55–67. [PubMed: 2001446]

19. Kemper, TL. Neuroanatomical and neuropathological changes during aging and dementia. In: Albert, MS.; Knoefel, JE., editors. Clinical Neurology and aging. New York: Oxford University Press; 1994. p. 3-67.

20. Ketonen LM. Neuroimaging of the aging brain. Neurol Clin 1998;16(3):581–598. [PubMed: 9666038]

21. Kikinis R, Shenton ME, Gerig G, Martin J, Anderson M, Metcalf D, Guttmann CR, McCarley RW, Lorensen W, Cline H, et al. Routine quantitative analysis of brain and cerebrospinal fluid spaces with MR imaging. J Magn Reson Imaging 1992;2(6):619–629. [PubMed: 1446105]

22. Kohn MI, Tanna NK, Herman GT, Resnick SM, Mozley PD, Gur RE, Alavi A, Zimmerman RA, Gur RC. Analysis of brain and cerebrospinal fluid volumes with MR imaging. Part I Methods, reliability, and validation. Radiology 1991;178(1):115–122. [PubMed: 1984289]

23. Krishnan KR, Husain MM, McDonald WM, Doraiswamy PM, Figiel GS, Boyko OB, Ellinwood EH, Nemeroff CB. In vivo stereological assessment of caudate volume in man: effect of normal aging. Life Sci 1990;47(15):1325–1329. [PubMed: 2233134]

24. Lai ZC, Moss MB, Killiany RJ, Rosene DL, Herndon JG. Executive system dysfunction in the aged monkey: spatial and object reversal learning. Neurobiol Aging 1995;16(6):947–954. [PubMed: 8622786]

25. Li ZH, Sun XW, Wang ZX, Zhang XC, Zhang da R, He S, Hu XP. Behavioral and functional MRI study of attention shift in human verbal working memory. Neuroimage 2004;21(1):181–191. [PubMed: 14741655]

26. Lintl P, Braak H. Loss of intracortical myelinated fibers: a distinctive age-related alteration in the human striate area. Acta Neuropathol (Berl) 1983;61(3–4):178–182. [PubMed: 6650131]

27. Mahut H, Zola-Morgan S, Moss M. Hippocampal resections impair associative learning and recognition memory in the monkey. J Neurosci 1982;2(9):1214–1220. [PubMed: 7119874]

28. Matochik JA, Chefer SI, Lane MA, Woolf RI, Morris ED, Ingram DK, Roth GS, London ED. Age-related decline in striatal volume in monkeys as measured by magnetic resonance imaging. Neurobiol Aging 2000;21(4):591–598. [PubMed: 10924777]

29. McDonald WM, Husain M, Doraiswamy PM, Figiel G, Boyko O, Krishnan KR. A magnetic resonance image study of age-related changes in human putamen nuclei. Neuroreport 1991;2(1):57–60. [PubMed: 1768851]

30. Meier-Ruge W, Ulrich J, Bruhlmann M M, Meier E. Age-related white matter atrophy in the human brain. Ann N Y Acad Sci 1992;673:260–269. [PubMed: 1485724]

31. Mishkin M. Memory in monkeys severely impaired by combined but not by separate removal of amygdala and hippocampus. Nature 1978;273(5660):297–298. [PubMed: 418358]

32. Moore TL, Killiany RJ, Herndon JG, Rosene DL, Moss MB. Impairment in abstraction and set shifting in aged rhesus monkeys. Neurobiol Aging 2003;24(1):125–134. [PubMed: 12493558]

33. Moore TL, Killiany RJ, Herndon JG, Rosene DL, Moss MB. A non-human primate test of abstraction and set shifting: An automated adaptation of the Wisconsin Card Sorting Test. J Neurosci Methods 2005;146(2):165–173. [PubMed: 16054506]

34. Morris ED, Chefer SI, Lane MA, Muzic RF Jr, Wong DF, Dannals RF, Matochik JA, Bonab AA, Villemagne VL, Grant SJ, Ingram DK, Roth GS, London ED. Loss of D2 receptor binding with age

in rhesus monkeys: importance of correction for differences in striatal size. J Cereb Blood Flow Metab 1999;19(2):218–229. [PubMed: 10027777]

35. Moss, M.; Albert, MS. Future directions in the study aging. In: Albert, MS.; Moss, M., editors. Geriatric Neuropsychology. New York and London: The Guilford Press; 1988. p. 293-303.
36. Moss MB, Rosene DL, Peters A. Effects of aging on visual recognition memory in the rhesus monkey. Neurobiol Aging 1988;9(5–6):495–502. [PubMed: 3062461]
37. Moss MB, Killiany RJ, Lai ZC, Rosene DL, Herndon JG. Recognition memory span in rhesus monkeys of advanced age. Neurobiol Aging 1997;18(1):13–19. [PubMed: 8983028]
38. Murphy DG, DeCarli C, Schapiro MB, Rapoport SI, Horwitz B. Age-related differences in volumes of subcortical nuclei, brain matter, and cerebrospinal fluid in healthy men as measured with magnetic resonance imaging. Arch Neurol 1992;49(8):839–845. [PubMed: 1343082]
39. Paxinos, G.; Huang, X-F.; Toga, A. The Rhesus Monkey Brain in Stereotaxic Coordinates. San Diego, CA: Academic Press; 1999.
40. Peters A, Rosene DL, Moss MB, Kemper TL, Abraham CR, Tigges J, Albert MS. Neurobiological bases of age-related cognitive decline in the rhesus monkey. J Neuropathol Exp Neurol 1996;55(8): 861–874. [PubMed: 8759775]
41. Peters A, Sethares C, Moss MB. The effects of aging on layer 1 in area 46 of prefrontal cortex in the rhesus monkey. Cereb Cortex 1998;8(8):671–684. [PubMed: 9863695]
42. Peters, A. Normal aging in the cerebral cortex of primates. In: Peters, A.; Morrison, JH., editors. Cerebral Cortex. New York: Kluwer Academic/Plenum Press; 1999. p. 49-80.
43. Pfefferbaum A, Mathalon DH, Sullivan EV, Rawles JM, Zipursky RB, Lim KO. A quantitative magnetic resonance imaging study of changes in brain morphology from infancy to late adulthood. Arch Neurol 1994;51(9):874–887. [PubMed: 8080387]
44. Pfefferbaum A, Desmond JE, Galloway C, Menon V, Glover GH, Sullivan EV. Reorganization of frontal systems used by alcoholics for spatial working memory: an fMRI study. Neuroimage 2001;14 (1 Pt 1):7–20. [PubMed: 11525339]
45. Presty SK, Bachevalier J, Walker LC, Struble RG, Price DL, Mishkin M, Cork LC. Age differences in recognition memory of the rhesus monkey (Macaca mulatta). Neurobiol Aging 1987;8(5):435–440. [PubMed: 3683724]
46. Rapp PR, Amaral DG. Evidence for task-dependent memory dysfunction in the aged monkey. J Neurosci 1989;9(10):3568–3576. [PubMed: 2795141]
47. Rapp PR, Amaral DG. Recognition memory deficits in a subpopulation of aged monkeys resemble the effects of medial temporal lobe damage. Neurobiol Aging 1991;12(5):481–486. [PubMed: 1770984]
48. Raz N, Torres IJ, Acker JD. Age, gender, and hemispheric differences in human striatum: a quantitative review and new data from in vivo MRI morphometry. Neurobiol Learn Mem 1995;63 (2):133–142. [PubMed: 7663886]
49. Raz N, Gunning FM, Head D, Dupuis JH, McQuain J, Briggs SD, Loken WJ, Thornton AE, Acker JD. Selective aging of the human cerebral cortex observed in vivo: differential vulnerability of the prefrontal gray matter. Cereb Cortex 1997;7(3):268–282. [PubMed: 9143446]
50. Raz N, Rodrigue KM, Kennedy KM, Head D, Gunning-Dixon F, Acker JD. Differential aging of the human striatum: longitudinal evidence. AJNR Am J Neuroradiol 2003;24(9):1849–1856. [PubMed: 14561615]
51. Raz N, Rodrigue KM, Head D, Kennedy KM, Acker JD. Differential aging of the medial temporal lobe: a study of a five-year change. Neurology 2004;62(3):433–438. [PubMed: 14872026]
52. Resnick SM, Pham DL, Kraut MA, Zonderman AB, Davatzikos C. Longitudinal magnetic resonance imaging studies of older adults: a shrinking brain. J Neurosci 2003;23(8):3295–3301. [PubMed: 12716936]
53. Salat DH, Kaye JA, Janowsky JS. Prefrontal gray and white matter volumes in healthy aging and Alzheimer disease. Arch Neurol 1999;56(3):338–344. [PubMed: 10190825]
54. Salat DH, Buckner RL, Snyder AZ, Greve DN, Desikan RS, Busa E, Morris JC, Dale AM, Fischl B. Thinning of the cerebral cortex in aging. Cereb Cortex 2004;14(7):721–730. [PubMed: 15054051]
55. Saunders RC, Aigner TG, Frank JA. Magnetic resonance imaging of the rhesus monkey brain: use for stereotactic neurosurgery. Exp Brain Res 1990;81(2):443–446. [PubMed: 2204546]

56. Tanna NK, Kohn MI, Horwich DN, Jolles PR, Zimmerman RA, Alves WM, Alavi A. Analysis of brain and cerebrospinal fluid volumes with MR imaging: impact on PET data correction for atrophy. Part II. Aging and Alzheimer dementia. Radiology 1991;178(1):123–130. [PubMed: 1984290]
57. Tigges J, Gordon TP, McClure HM, Hall EC, Peters A. Survival rate and life span of the rhesus monkey. American Journal of Primatology 1988;(15):263–273.
58. Warfield S, Dengler J, Zaers J, Guttmann CR, Wells WM 3rd, Ettinger GJ, Hiller J, Kikinis R. Automatic identification of gray matter structures from MRI to improve the segmentation of white matter lesions. J Image Guid Surg 1995;1(6):326–338. [PubMed: 9080353]
59. Wei X, Warfield SK, Zou KH, Wu Y, Li X, Guimond A, Mugler JP 3rd, Benson RR, Wolfson L, Weiner HL, Guttmann CR. Quantitative analysis of MRI signal abnormalities of brain white matter with high reproducibility and accuracy. J Magn Reson Imaging 2002;15(2):203–209. [PubMed: 11836778]
60. Wells WM 3rd, Grimson WEL, Kikinis R, Jolesz FA. Statistical intensity correction and segmentation of MRI data. SPIE, Visualization in Biomedical Computing 1994;Volume 2359:13–24.
61. Wells WM 3rd, Grimson WEL, Kikinis R, Jolesz FA. Adaptive segmentation of MRI data. IEEE Transactions on Medical Imaging 1996;(15):429–442. [PubMed: 18215925]
62. Yeterian EH, Pandya DN. Striatal connections of the parietal association cortices in rhesus monkeys. J Comp Neurol 1993;332(2):175–197. [PubMed: 8331211]
63. Yeterian EH, Pandya DN. Corticostriatal connections of the superior temporal region in rhesus monkeys. J Comp Neurol 1998;399(3):384–402. [PubMed: 9733085]

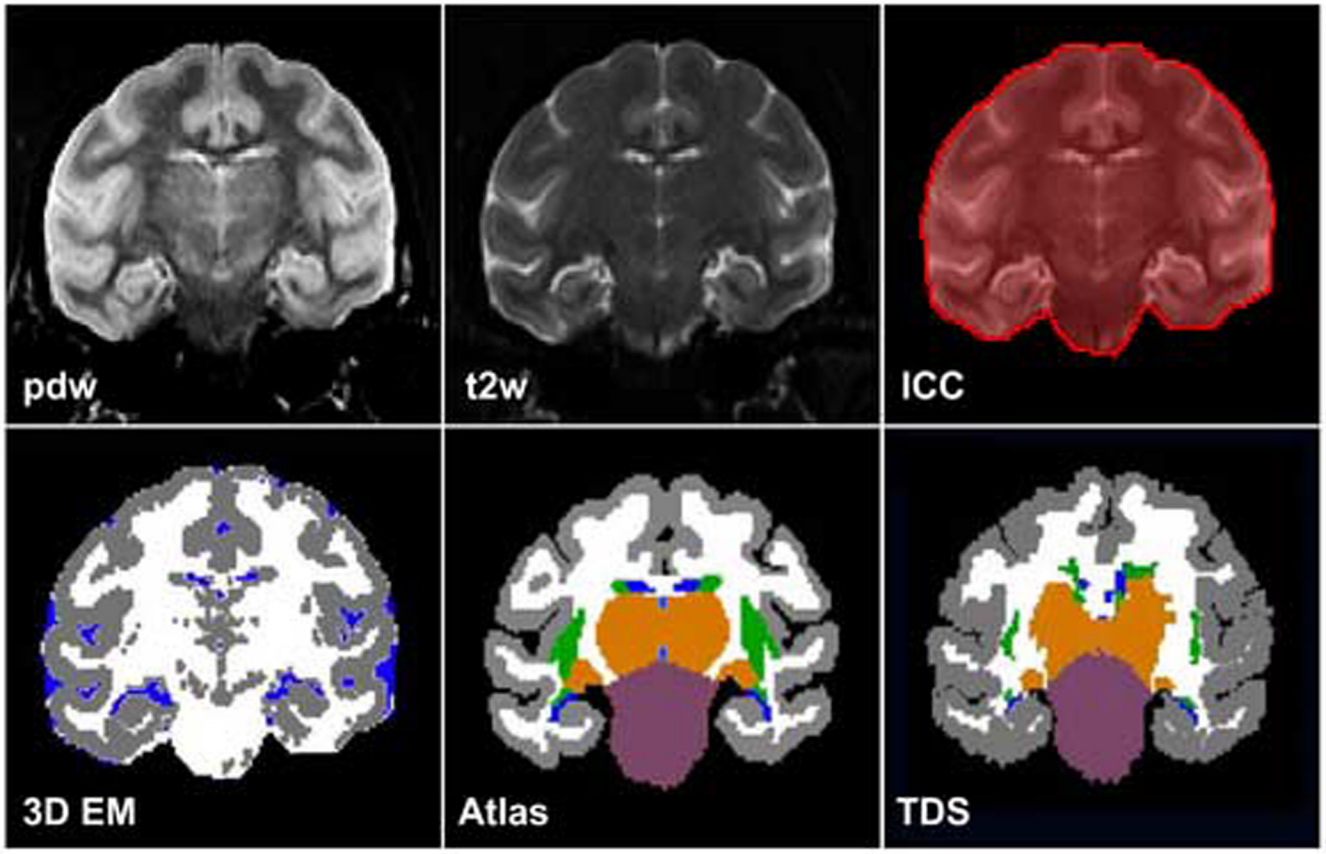

Figure 1.

Automated segmentation procedure. Interleaved proton density weighted (pdw) and T2-weighted images (T2w) served as the input for the segmentation pipeline. An intracranial cavity mask (ICC) was created, separating "brain" from "non-brain voxels." Brain voxels were segmented into gray matter, white matter and CSF classes using the 3D Expectation-Maximization (3D EM) algorithm. An *a priori* atlas (Atlas) containing 14 regions of interest (ROI's) segmented from a dual-echo spin-echo (DE SE) data set of a young (7 years old), behaviorally normal monkey (AM093) was created and then elastically matched to the 3D EM results to produce an anatomically based segmentation (TDS) of the gray matter, white matter and CSF voxels. The ROI's included forebrain white matter, cerebral cortex, caudate nucleus, putamen, globus pallidus, claustrum, thalamus, hypothalamus, brainstem, cerebellum, lateral ventricles, third ventricle, cerebral aqueduct and fourth ventricle, whose operational definitions are made explicit in the Appendix. Colors for "3D EM": Gray = gray matter; White = white matter; Blue = CSF. Colors for "Atlas" and "TDS": Gray = cortical gray matter; White = forebrain white matter; Blue = ventricles; Green = basal ganglia structures (caudate nucleus, putamen, globus pallidus, claustrum, each analyzed separately); Orange = thalamus; Purple = brainstem.

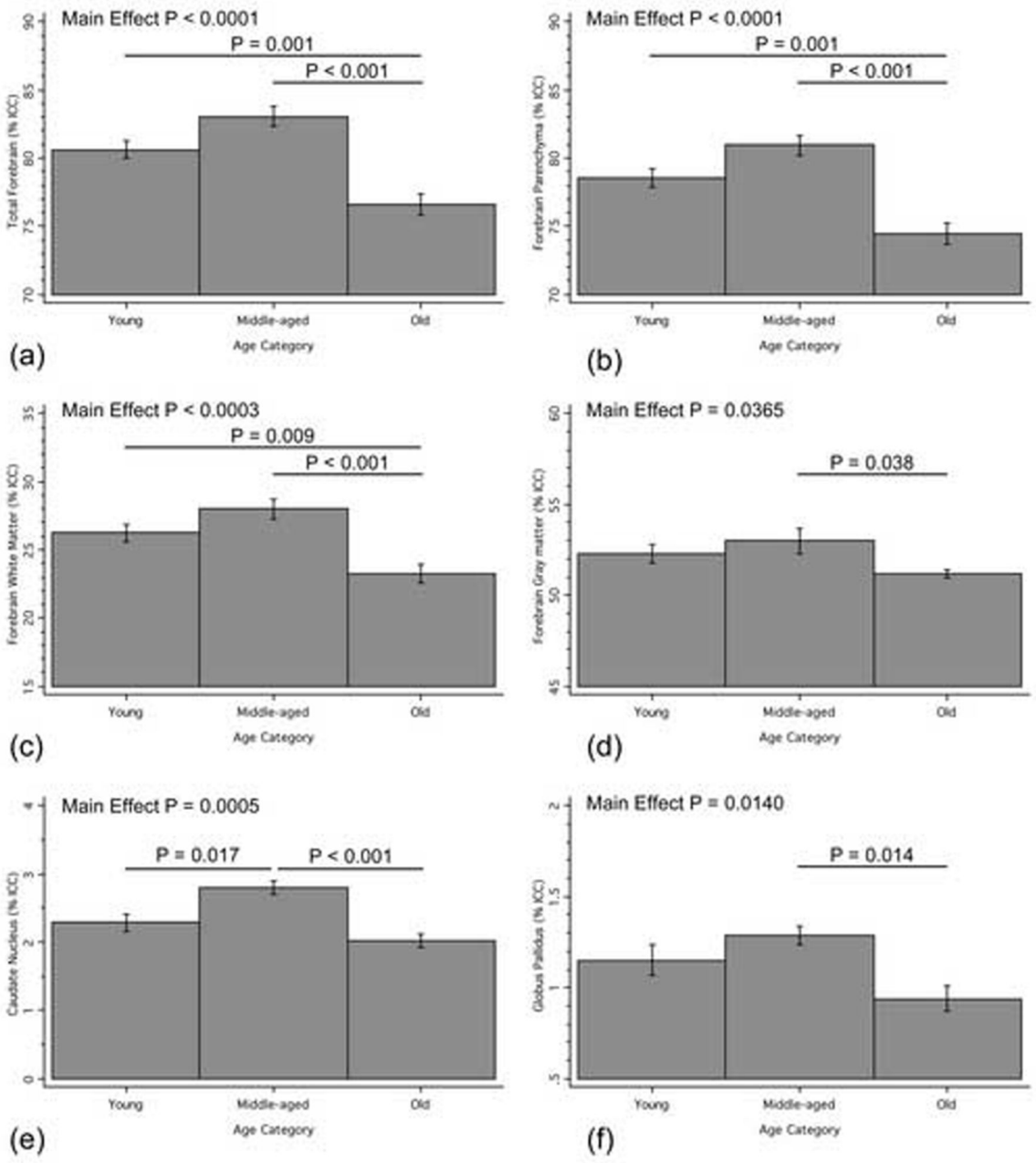

Figure 2.

Standardized ROI volume for total forebrain (a), forebrain parenchyma (b), forebrain white matter (c), forebrain gray matter (d), caudate nucleus (e) and globus pallidus (f) as a function of age category. Bars and P-values indicate significant changes between cohorts.

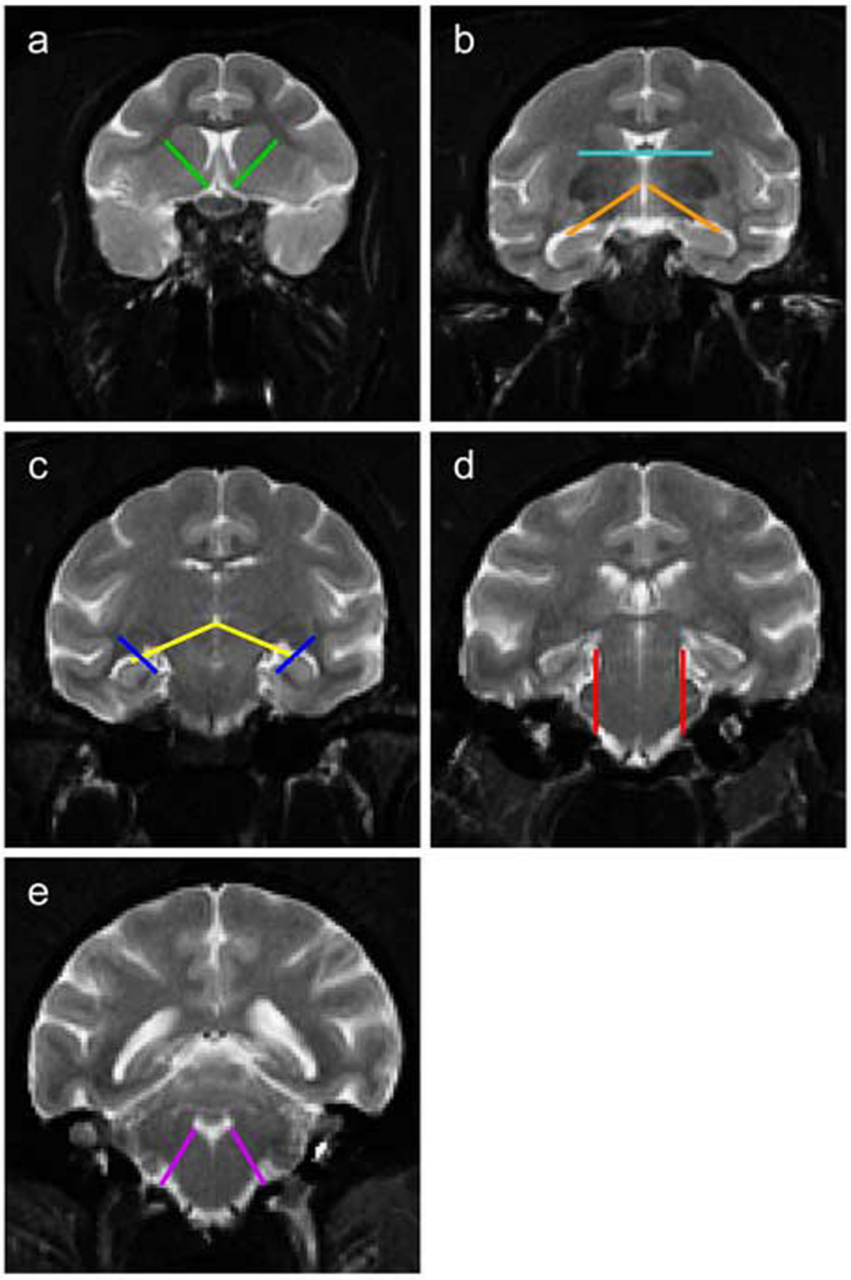

Figure A1.
Reference landmarks used to operationally define borders of regions of interest (ROI's). The image slices shown here are representative of several slices in which the landmark was used by manual raters. Landmarks: caudate-putamen (a), third ventricle and thalamus-hypothalamus (b), thalamus-brainstem and lateral ventricle (c), brainstem-cerebellum (d), fourth ventricle (e).

Table 1

Animal subjects age, age at scan and behavioral scores. Mean (SE) are summarized at the bottom of each age group. Abbreviations: Delayed Non-Matching to Sample (DNMS), Delayed Recognition Span Task (DRST), Cognitive Impairment Index (CII).

			Behavioral Measures					
Age Category	**Age at Scan**	**Age at Testing Criterion**	**DNMS Acquisition (errors)**	**DNMS 2-min (% correct)**	**DNMS 10-min (% correct)**	**DRST spatial (span)**	**DRST object (span)**	**CII**
Young	5							
Young	6							
Young	7	7	45	88	77	2.64	5.31	−0.09
Young	7	7	62	82	78	2.85	5.32	0.34
Young	10	8	71	93	82	2.06	3.39	0.3
Young	10	8	52	83	79	1.9	2.75	0.9
Young	10							
Young	12	10	60	92	87	2.18	3.19	0.17
Mean (SE)	8.38 (0.86)	8.00 (0.55)	58.00 (4.44)	87.60 (2.25)	80.60 (1.81)	2.33 (0.18)	3.99 (0.55)	0.32 (0.16)
Middle-Aged	16	16	6			2.22	4.49	
Middle-Aged	16							
Middle-Aged	16	16	238			2.32	3.26	
Middle-Aged	17	17	114	56		1.82	1.38	4.21
Middle-Aged	17	17	16	90				
Middle-Aged	19	19	97	85	67	2.32	3.79	0.94
Mean (SE)	16.83 (0.48)	17.00 (0.55)	94.20 (41.82)	77.00 (10.60)	67.00	2.17 (0.12)	3.23 (0.67)	2.58 (1.64)
Old	24	22	151	90		2.17	2.6	1.34
Old	24	21	77	90	77	2.26	3.79	0.43
Old	25	21	60	79	60	2.11	3.48	1.09
Old	27	24	353	90		1.93		3.81
Old	30	29	70			2.59	3.03	
Old	30	30	29	88	70	2.2	3.42	
Old	30	26	98	94		1.84		0.73
Old	30							
Mean (SE)	27.50 (1.00)	24.71 (1.41)	119.71 (41.39)	88.50 (2.06)	69.00 (4.93)	2.16 (0.09)	3.26 (0.21)	1.48 (0.60)

Table 2

Mean (SE) of standardized ROI volumes according to age group. Significant volume changes between young and old age (*), between middle-age and old age (#) and between young and middle-age (+) are indicated with the ROI name.

	Regions of Interest (ROI)				
Age Category	**Total Forebrain*#**	**Forebrain Parenchyma*#**	**Forebrain White Matter*#**	**Forebrain Gray Matter#**	**Cerebral Cortex**
Young	80.61 (0.64)	78.54 (0.68)	26.25 (0.67)	52.28 (0.53)	41.66 (0.61)
Middle-Aged	83.06 (0.57)	80.96 (0.59)	27.98 (0.56)	52.98 (0.56)	42.36 (0.44)
Old	76.57 (0.81)	74.42 (0.80)	23.23 (0.68)	51.19 (0.21)	41.58 (0.25)
	Caudate Nucleus+#	Putamen	Globus Pallidus#	Claustrum	
Young	2.29 (0.13)	2.65 (0.14)	1.15 (0.09)	0.54 (0.01)	
Middle-Aged	2.81 (0.08)	2.41 (0.16)	1.29 (0.04)	0.50 (0.03)	
Old	2.02 (0.11)	2.34 (0.12)	0.94 (0.07)	0.57 (0.02)	
	Thalamus	Hypothalamus	Brainstem	Cerebellum	
Young	3.81 (0.29)	0.18 (0.03)	3.40 (0.16)	9.56 (0.41)	
Middle-Aged	3.43 (0.21)	0.18 (0.02)	3.26 (0.31)	9.65 (0.55)	
Old	3.52 (0.15)	0.23 (0.02)	3.27 (0.09)	8.74 (0.43)	
	Ventricular CSF	Lateral Ventricles	Third Ventricle	Cerebral Aqueduct	Fourth Ventricle
Young	2.08 (0.08)	1.73 (0.07)	0.12 (0.02)	0.06 (0.00)	0.16 (0.01)
Middle-Aged	2.10 (0.06)	1.80 (0.06)	0.08 (0.01)	0.06 (0.02)	0.15 (0.02)
Old	2.15 (0.06)	1.79 (0.07)	0.17 (0.02)	0.06 (0.01)	0.14 (0.01)